www.nature.com/mi

MucosalImmunology

ARTICLE OPEN

Regulation of HMGB1 release protects chemoradiotherapy-associated mucositis

Keon-Il Im[1,2], Young-Sun Nam[1,2], Nayoun Kim[1,2], Yunejin Song[1,2], Eun-Sol Lee[1,2], Jung-Yeon Lim[1,2], Young-Woo Jeon[1,2,3] and Seok-Goo Cho[1,2,3]

Oral mucositis (OM) is a common complication in cancer patients undergoing anticancer treatment. Despite the clinical and economic consequences of OM, there are no drugs available for its fundamental control. Here we show that high-mobility group box 1 (HMGB1), a "danger signal" that acts as a potent innate immune mediator, plays a critical role in the pathogenesis of OM. In addition, we investigated treatment of OM through HMGB1 blockade using NecroX-7 (tetrahydropyran-4-yl)-[2-phenyl-5-(1,1-dioxo-thiomorpholin-4-yl)methyl-1Hindole-7-yl]amine). NecroX-7 ameliorated basal layer epithelial cell death and ulcer size in OM induced by chemotherapy or radiotherapy. This protective effect of NecroX-7 was mediated by inhibition of HMGB1 release and downregulation of mitochondrial oxidative stress. Additionally, NecroX-7 inhibited the HMGB1-induced release of tumor necrosis factor-alpha (TNF-α), interleukin (IL)-1β, and macrophage inflammatory protein (MIP)-1β, as well as the expression of p53-upregulated modulator of apoptosis (PUMA) and the excessive inflammatory microenvironment, including nuclear factor-kB (NF-kB) pathways. In conclusion, our findings suggest that HMGB1 plays a key role in the pathogenesis of OM; therefore, blockade of HMGB1 by NecroX-7 may be a novel therapeutic strategy for OM.

Mucosal Immunology (2019) 12:1070–1081; https://doi.org/10.1038/s41385-019-0132-x

INTRODUCTION

Oral mucositis (OM) is a devastating side effect in hematopoietic stem cell transplant (HSCT) settings, and in patients undergoing chemotherapy or radiotherapy for cancer treatment.[1,2] Despite the clinical and economic consequences of OM, oral irrigation to prevent secondary bacterial infections or pain relief by narcotic analgesics is currently the only treatment option in clinical practice. While palifermin, a recombinant human keratinocyte growth factor approved by the US Food and Drug Administration (FDA),[3,4] is available, its application is greatly limited by its ineffectiveness against tumors other than hematological malignancies and high costs due to the requirement for frequent injections.

Activation of WNT/β-catenin pathways, including Rspondin1,[5–7] growth factors,[8] and LGR5 receptor agonists[9,10] has been proposed as the treatment strategy to regenerate progenitor and stromal cells in mucosal injury, and radioprotective agents including mTOR inhibitors[8] and amifostine[11] have been proposed to prevent OM. In addition, Han et al. reported that smad7 blocks transforming growth factor-induced apoptosis and growth arrest, and plays a key role in inhibiting the inflammatory response due to nuclear factor κB (NF-κB) activation.[12] However, few drugs for control of OM are available.

Tissue damage by radiotherapy and chemotherapy results in the release of pathogen-associated molecular patterns (PAMPs), which function as pro-inflammatory agents, and of danger-associated molecular patterns (DAMPs).[13,14] Together, PAMPs and DAMPs activate the innate immune system by interacting with pattern-recognition receptors, Toll-like receptors (TLRs), and NOD-like receptors, and subsequently amplify the acute inflammatory response by acting as a secondary signal transduction system.[15] An activated innate immune response plays a key role in the pathophysiology of OM.[16]

High-mobility group box 1 (HMGB1) in the cytoplasm functions as a typical DAMP and is involved in the pathogenesis of various diseases.[13,17,18] Other than its internal receptor RAGE, HMGB1 also directly binds to TLRs, which are also PAMP receptors. In addition, excessive conditioning regimens, such as total body irradiation (TBI) and chemotherapy, damage host tissue and the damaged cells secrete HMGB1.[19,20] Thus, the hypothesis of this study was that HMGB1 is a key mechanism of OM caused by radiotherapy and chemotherapy, and reducing the HMGB1 level could ameliorate OM.

NecroX (cyclopentylamino carboxymethylthiazolylindole) is a class of indole-derived cell-permeable, mitochondrial-targeted antioxidant molecules that exhibit anti-inflammatory and anti-necrotic effects.[21] Furthermore, NecroX restores dysfunctional human immunodeficiency virus-specific CD8+ T-cell proliferation[22] and RIPK1-RIPK3-induced necroptosis caused by mitochondrial reactive oxygen species (ROS).[23] A phase I clinical trial involving healthy adult males confirmed that a single intravenous (i.v.) dose of NecroX-7 is safe and well tolerated up to 200 mg.[24] Moreover, as well as inhibiting the passive release of HMGB1 from necrotic cells due to excessive conditioning regimens, NecroX-7 also blocks active secretion of HMGB1 from immunologically activated immune cells.[25] The ability of NecroX-7 to suppress necroptosis and HMGB1 provides a rationale for its use in OM.

[1]Institute for Translational Research and Molecular Imaging, Catholic Institutes of Medical Science, Seoul, Korea; [2]Laboratory of Immune Regulation, Convergent Research Consortium for Immunologic Disease, Seoul St. Mary's Hospital, Seoul, Korea and [3]Department of Hematology, Catholic Blood and Marrow Transplantation Center, Seoul St. Mary's Hospital, The Catholic University of Korea College of Medicine, Seoul, Korea
Correspondence: S.-G. Cho (chosg@catholic.ac.kr)

Received: 25 April 2018 Revised: 28 November 2018 Accepted: 31 December 2018
Published online: 15 January 2019

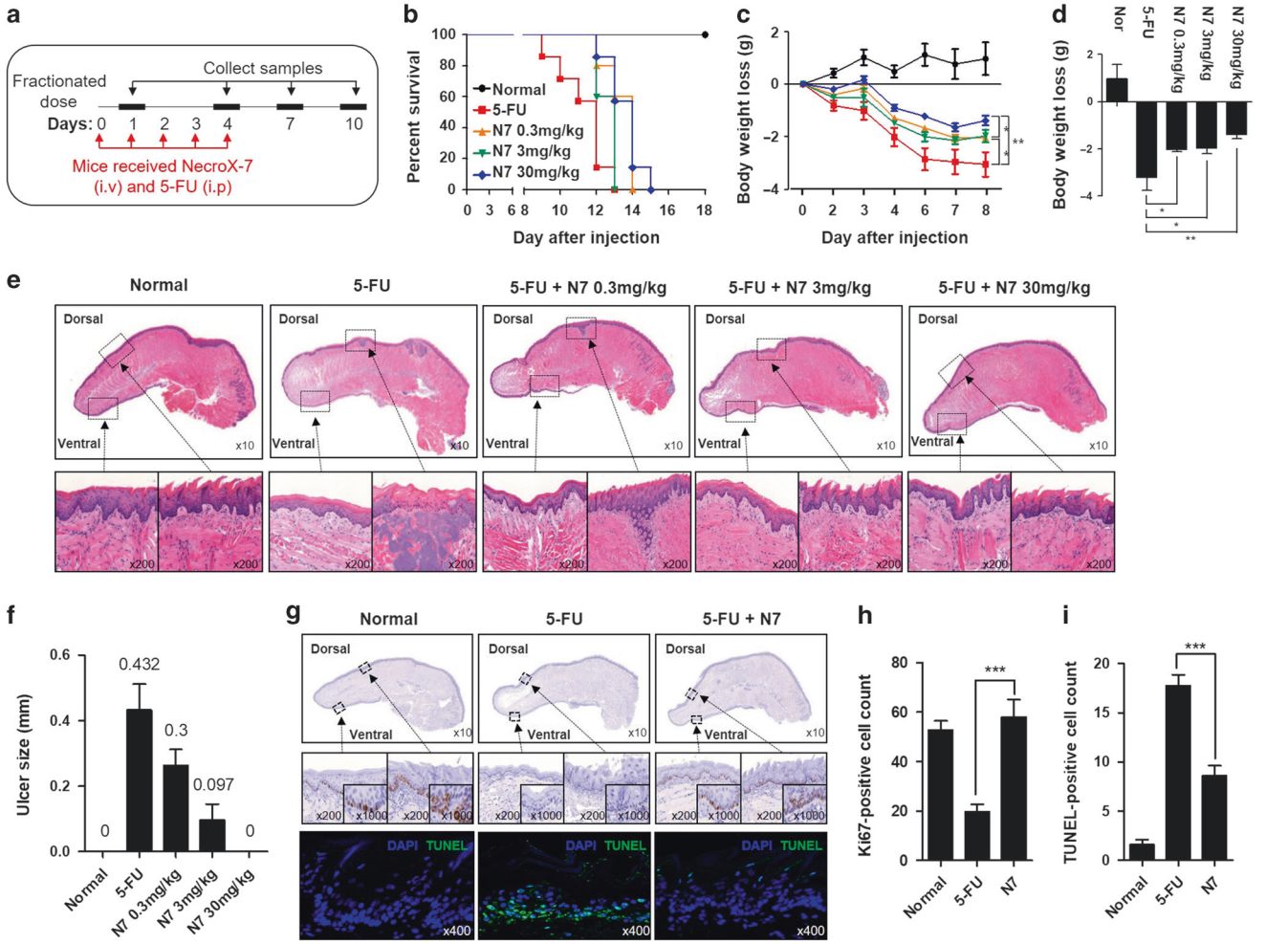

Fig. 1 NecroX-7 prevents chemotherapy-induced oral mucositis (OM) in mice. **a** High-dose chemotherapy-induced mouse model of OM and drug treatment. Mice were administered 5-fluorouracil (5-FU; 50 mg/kg, intraperitoneally [i.p.]) once daily for 5 days (days 0–4) to induce OM. NecroX-7 (0.3, 3, and 30 mg/kg, intravenously [i.v.]) or phosphate-buffered saline was administered once daily for 5 days. **b** Kaplan-Meier survival curve of mice subjected to 5-FU. **c** Body weight loss (%) was measured daily, and **d** data were analyzed on day 8. **e** Morphological changes were evaluated by H & E staining, and **f** ulcer size was measured on day 10 after initiation of 5-FU treatment. **g** Representative immunohistochemical staining for proliferation of mucosal epithelial cells was measured by Ki67 staining (brown, upper panel) and apoptosis of mucosal epithelial cells was assessed by terminal deoxynucleotidyl transferase-dUTP nick-end labeling (TUNEL) staining (green, lower panel). **h**, **i** Quantification (mean ± standard deviation) of Ki67 and TUNEL-positive cell count in **g**. N7 NecroX-7. Results are representative of three independent experiments ($n = 8$ mice/group). $^{*}P < 0.05$, $^{**}P < 0.01$, $^{***}P < 0.001$

Here we suggest that HMGB1, a "danger signal" that acts as a potent innate immune mediator, plays a critical role in the pathogenesis of OM. In addition, blockade of HMGB1 by NecroX-7 significantly attenuated OM-related basal layer epithelial cell death, reduced ulcer size, and decreased activation of inflammatory pathways. Therefore, NecroX-7 has potential as a novel therapeutic strategy for OM in cancer patients.

RESULTS

NecroX-7 prevents the deleterious effects of chemotherapy on tongue mucosa cellularity

The efficacy of mitochondrial-targeted NecroX-7 was evaluated using a chemotherapy-induced OM model. Seven-week-old B6 mice received 5-fluorouracil (FU) for chemotherapy for 5 consecutive days and, before each administration of 5-FU, mice were injected with saline (control) or NecroX-7 (0.3, 3, and 30 mg/kg) (Fig. 1a). The chemical structure of NecroX-7 is shown in Supplementary Figure 1a. Efficacy was evaluated in triplicate for each dose, and representative results are shown in Fig. 1. Clinically, we observed that NecroX-7 improved survival in mice exposed to 5-FU-induced toxicity (Fig. 1b). We also observed continuous body weight loss in the group without NecroX-7 treatment, which peaked on day 7 and began to recover on day 8 (Fig. 1c). The body weight loss was significantly decreased in the NecroX-7 treatment group on day 8 in a dose-dependent manner (Fig. 1d). Next, we examined OM pathology in tongue tissue at 10 days after chemotherapy. Histopathologically, hematoxylin and eosin (H & E) staining showed that untreated mucosa displayed complete atrophy of the epithelial surface, including ulceration of the mucosal lining, disruption of the epithelial layer, and loss of the basal membrane (Fig. 1e). However, treatment with NecroX-7 decreased the severity and incidence of ulceration in a dose-dependent manner (Fig. 1f) and restored the thickness of the epithelial layer as compared with the untreated control group (Fig. 1e). Consistent with the above observations, analysis of Ki67- and terminal deoxynucleotidyl transferase-dUTP nick-end labeling (TUNEL)-stained ventral and dorsal tongue sections confirmed the

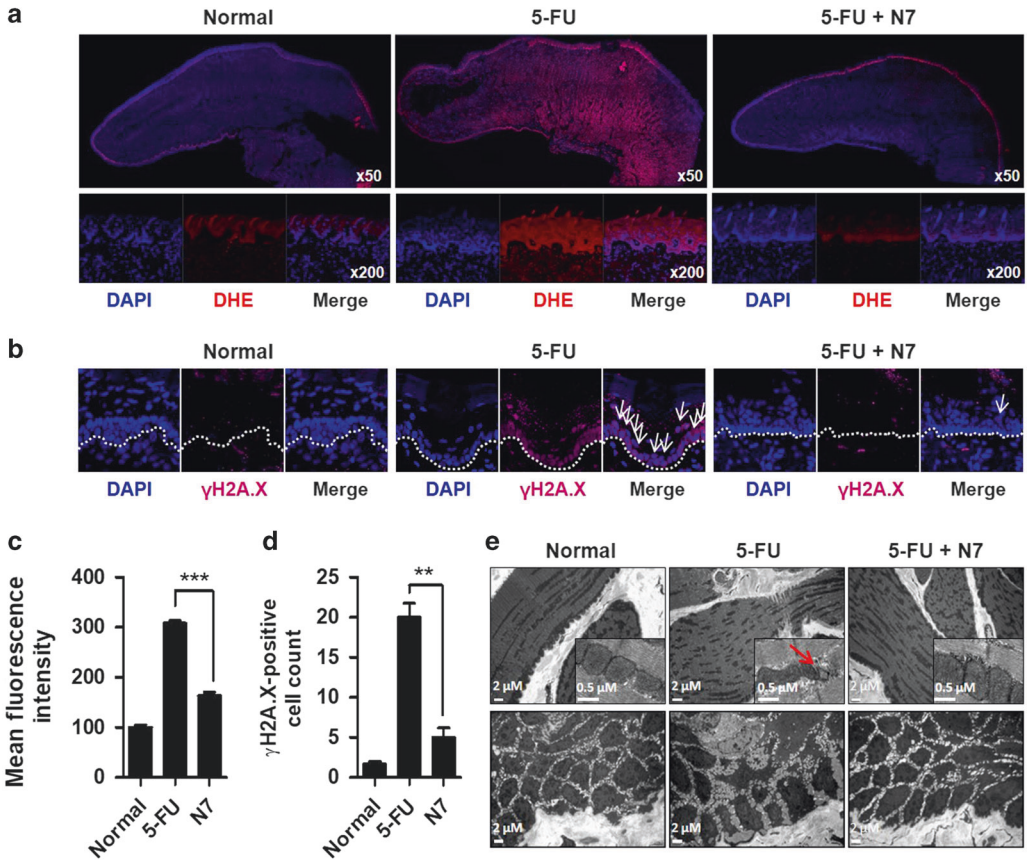

Fig. 2 NecroX-7 reduced oxidative stress, mitochondrial dysfunction, and apoptosis in 5-fluorouracil (5-FU)-induced oral mucositis (OM). Reactive oxygen species (ROS) accumulation in chemotherapy-induced OM. **a** Representative fluorescence photomicrographs of sections of mouse tongue mucosa labeled with dihydroethidium (DHE; red) and counterstained with 4′,6-diamidino-2-phenylindole (DAPI; blue) to show nuclei. DHE fluorescence intensity is shown. The NecroX-7-treated group showed significantly reduced ROS levels. Original magnification, ×50 and ×200. **b** Representative confocal images of γH2AX (red) staining in the ventral tongue. Blue, DAPI. Arrows indicate rH2A.X+ cells, and numbers of foci in epithelial cells are plotted. **c**, **d** Quantification of the staining in **a** and **b**. **e** Transmission electron microscopy analysis of mitochondrial morphology in the tongue of vehicle- or NecroX-7-treated mice with OM. The NecroX-7-treated group exhibited reduced mitochondrial dysfunction and apoptosis. Arrows indicate abnormal mitochondria. Scale bars, 0.5 and 100 μm. N7 NecroX-7. $^{**}P < 0.01$, $^{***}P < 0.001$

protective effect of NecroX-7 against chemotherapy-induced OM (Fig. 1g). A high dose of 5-FU reduced mucosal basal layer epithelial cellularity and increased epithelial cell apoptosis in the tongue mucosa (Fig. 1g). In contrast, NecroX-7 treatment significantly increased basal layer epithelial cellularity and inhibited epithelial cell apoptosis in the tongue mucosa (Fig. 1h, i). These results demonstrate that NecroX-7 prevents reduction in epithelial cell proliferative capacity and is effective against chemotherapy-induced mucosal injury.

NecroX-7 suppresses ROS and γH2AX levels in tongue tissue

OM can lead to enhanced oxidative stress and mitochondrial damage, resulting in apoptosis.[16,26] Therefore, we evaluated oxidative stress levels using the ROS detection dye dihydroethidium. Indeed, chemotherapy significantly increased ROS levels in the tongue (Fig. 2a), which correlated with a marked increase in the number of cells expressing the DNA damage response marker γ-H2AX (Fig. 2b). Additionally, NecroX-7 suppressed the levels of ROS and γH2AX (Fig. 2c, d), indicating that NecroX-7 protects normal epithelial cells against DNA damage and oxidative stress. Next, we used electron microscopy to analyze mitochondrial structure. Mitochondria in the tongue tissues of chemotherapy-treated mice were largely decreased or shattered, but these effects were ameliorated by NecroX-7 (Fig. 2e). These findings indicate that the protective effect of NecroX-7 against mitochondrial-dependent apoptosis is mediated by suppression of ROS production.

NecroX-7 attenuates HMGB1 accumulation in the tongue mucosa

In our previous study, we found that immune cells stimulated with H_2O_2 translocate HMGB1 from the nucleus to the cytoplasm, followed by extracellular transport.[25] This suggests that excessive ROS activation is the main cause of accelerated HMGB1 secretion. Consistent with these findings, severe oxidative stress resulted in increased levels of key proteins, such as HMGB1, as determined by polymerase chain reaction (PCR) (Fig. 3a). The HMGB1 mRNA level peaked on day 7 after chemotherapy, and there were indications of a direct correlation between HMGB1 levels and the severity of OM. In addition, administration of NecroX-7 significantly reduced these levels (Fig. 3a). Immunohistochemical (IHC) staining showed that translocated HMGB1 (normally located in the nucleus) is increased in oral mucosa (located in the cytoplasm) (Fig. 3b). Also, the percentage of epithelial cells with only cytoplasmic HMGB1 staining among all epithelial cells was calculated on day 10. The cytoplasmic HMGB1 levels were significantly increased in the presence of chemotherapy-induced oral mucosa, but NecroX-7 application led to retention of HMGB1 staining in the nucleus (Fig. 3c). These results suggest that HMGB1 is involved in the

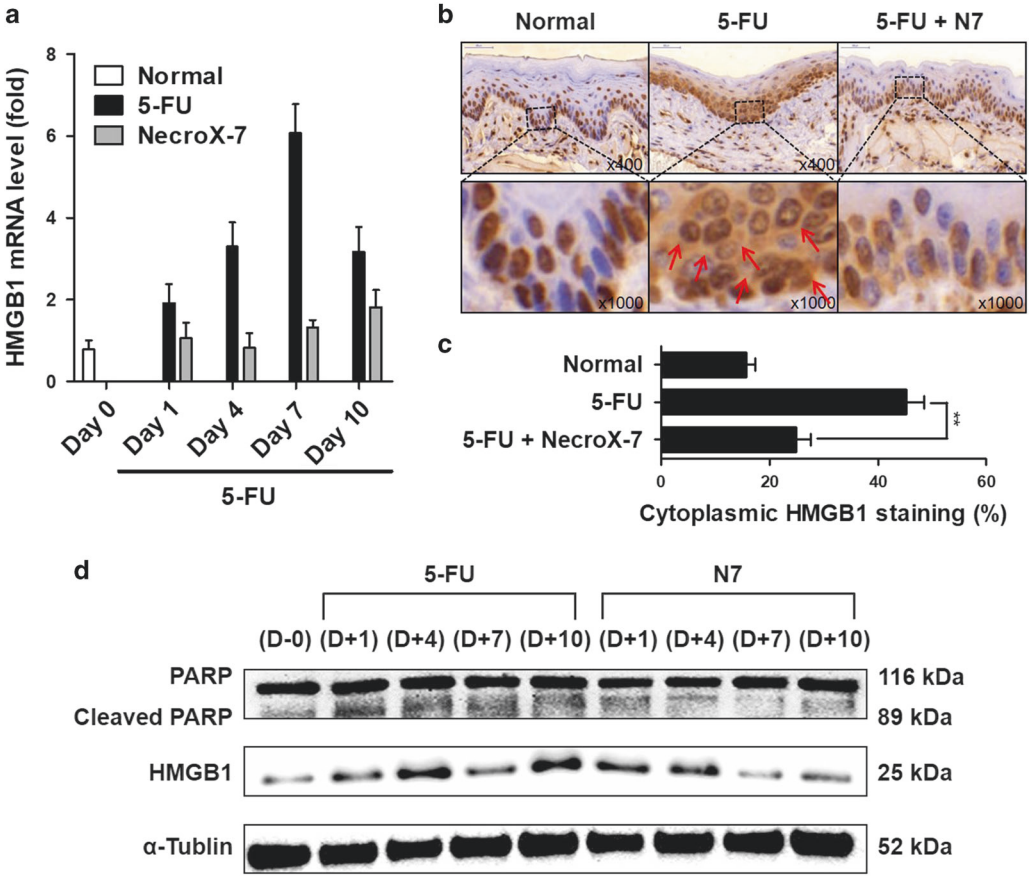

Fig. 3 High-mobility group box 1 (HMGB1) inhibition by NecroX-7 protected chemotherapy-induced mucositis. Mice were euthanized 1, 4, 7, and 10 days after the first injection of 5-fluorouracil (5-FU) and tongue tissues were collected for analysis. **a** HMGB1 mRNA levels were measured at the indicated times by real-time polymerase chain reaction using β-actin for normalization. **b** HMGB1 translocation. HMGB1 localization was visualized by immunohistochemistry. Brown, HMGB1; blue, nuclei stained with hematoxylin; arrows indicate cytoplasmic HMGB1 staining. The two black boxes in the upper panels (×400) are shown at higher magnification in the lower panels (×1000). **c** The percentage of immune cells with only cytoplasmic HMGB1 staining among total number of tissues was calculated. Representative images from six mice per group are shown. **d** Poly-ADP-ribose polymerase (PARP) and HMGB1 levels were analyzed by western blotting, using α-tubulin as the loading control. Two independent experiments were performed. N7 NecroX-7. $^{**}P < 0.01$

pathogenesis of chemotherapy-induced OM. Next, to determine whether inhibition of HMGB1 release ameliorates OM, we evaluated the levels of apoptosis-related proteins by western blot. Interestingly, inhibition of HMGB1 release by NecroX-7 suppressed apoptosis, as determined by cleaved poly-ADP-ribose polymerase (PARP) assay (Fig. 3d). Taken together, these data suggest that NecroX-7 protects against OM by reducing HMGB1 accumulation in the tissues.

NecroX-7 decreases HMGB1 and p53-upregulated modulator of apoptosis release

To determine whether HMGB1 release is associated with cell death during chemotherapy, we evaluated the levels of apoptosis-related proteins and genes. p53/PUMA is the major mediator of chemotherapy-induced mucosal injury.[27,28] Previous studies have demonstrated that p53 phosphorylation induces pro-apoptotic genes such as Bcl-2-associated X protein (*Bax*) and p53-upregulated modulator of apoptosis (*PUMA*).[29] Our data indicated that 5-FU-induced OM significantly induced p53 phosphorylation (Fig. 4a) and PUMA (Fig. 4b) and Bax expression (Fig. 4d), as well as PARP cleavage, resulting in mucosal cell apoptosis. We then further investigated the potential regulation of the p53-dependent apoptosis pathway by NecroX-7. Western blotting and PCR analysis showed that the administration of NecroX-7 abolished p53 phosphorylation, subsequently protecting against PARP cleavage (Fig. 4a), and reduced PUMA and Bax expression compared with untreated tongue tissues (Fig. 4b, d). We used IHC staining to confirm a decrease in the expression of cytoplasmic p53, but not in that of nuclear p53 (Fig. 4c). Furthermore, NecroX-7 restored the Bax/Bcl ratio and caspase-3 to normal in tongue tissue (Fig. 4d). Taken together, these results suggest that the inhibition of HMGB1 by NecroX-7 suppresses p53 activation and its translocation to the cytoplasm, and regulates PUMA/Bax-mediated cell death pathways.

NecroX-7 prevents nuclear translocation of NF-κB p65 in the tongue mucosa

NF-κB activation and translocation occur in the tongue tissue of patients with OM caused by radiation or chemotherapeutics.[12] The level of nuclear NF-κB p65 in tongue tissues of mice with high-dose chemotherapy-induced OM was significantly increased compared with that in normal mice (Fig. 5a). In addition, the increase in the nuclear NF-κB p65 level was significantly reduced by administration of NecroX-7 (Fig. 5b). Next, we performed quantitative real-time PCR of TNF-α and IL-1β mRNA levels in the tongue tissue. The TNF-α and IL-1β levels were significantly increased in mice with chemotherapy-induced OM, but were significantly decreased in NecroX-7-injected mice (Fig. 5c). The serum levels of TNF-α, IL-1β, macrophage inflammatory protein (MIP)-1β, and IL-18 in mice with chemotherapy-induced mucositis were markedly increased compared with those in normal mice (Fig. 5d). Administration of NecroX-7 significantly reduced these

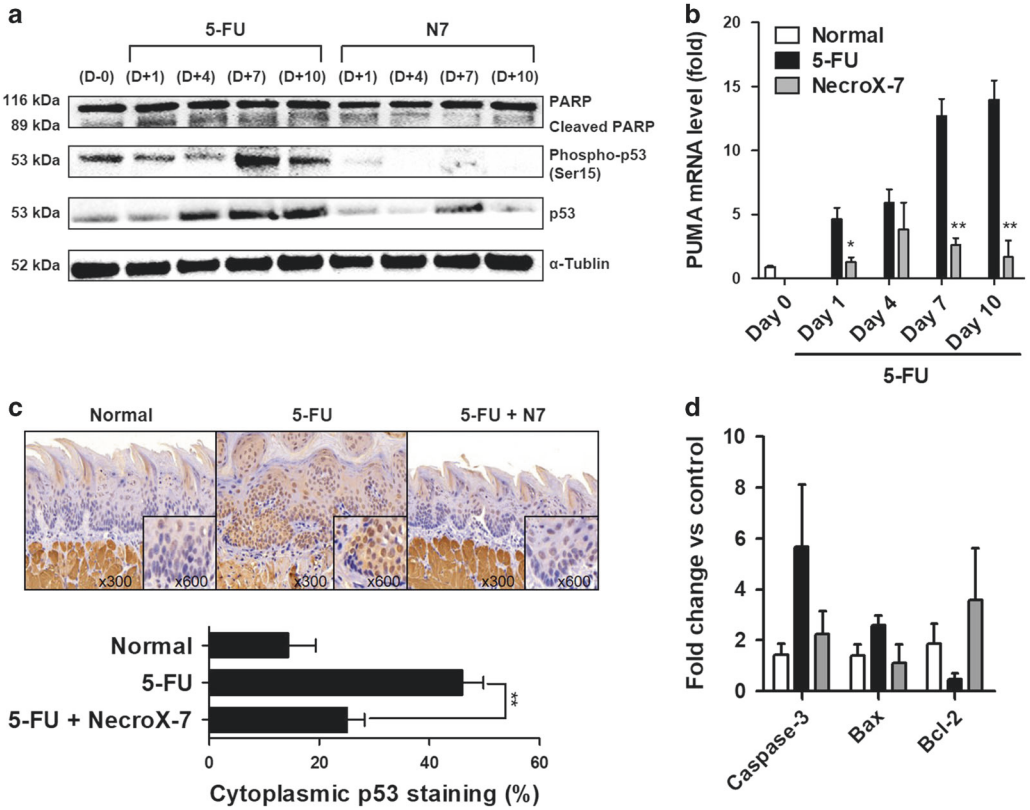

Fig. 4 NecroX-7 protect oral mucositis from increased high-mobility group box 1 (HMGB1) release and p53-upregulated modulator of apoptosis (PUMA). Mice were euthanized 1, 4, 7, and 10 days after the first injection of 5-fluorouracil (5-FU) and tongue tissues were collected for analysis. **a** Phospho-p53 (Ser15) and p53 protein levels analyzed by western blotting, using α-tubulin as the loading control. Two independent experiments were performed. **b** PUMA mRNA levels were measured at the indicated times by real-time polymerase chain reaction using β-actin for normalization. **c** p53 localization was visualized by immunohistochemistry. Brown, p53; blue, nuclei stained with hematoxylin. Original magnification, ×300 and ×600. **d** Caspase-3, Bax, and Bcl-2 expression levels were determined in tongue tissues by real-time PCR using β-actin for normalization. N7 NecroX-7. $^{*}P < 0.05$, $^{**}P < 0.01$

increases in TNF-α, IL-1β, MIP-1β, and IL-18 levels (Fig. 5d). Conversely, administration of NecroX-7 significantly reversed the decrease in the granulocyte-macrophage colony-stimulating factor (GM-CSF) level, but did not affect that of vascular endothelial growth factor-A (VEGF-A). These findings indicate that NecroX-7 ameliorates excessive inflammation by blocking production of pro-inflammatory cytokines and activation of the NF-κB pathway.

NecroX-7 protect against radiation- and chemotherapy-induced OM but not *N*-acetylcysteine

To assess the therapeutic potential of NecroX-7 in a representative model of human OM, we established a mouse model of OM induced by chemotherapy and radiotherapy (Fig. 6a). While the combination of 5-FU and 8 Gy radiation significantly reduced epithelium thickness from 50.2 to 20.2 μm, NecroX-7 treatment markedly increased the epithelial thickness of the ventral tongue, to 40.5 μm (Fig. 6b, c). We next compared the protective effect of NecroX-7 with that of *N*-acetylcysteine (NAC). NecroX-7 resulted in greater amelioration of epithelium disruption than 200 mg/kg NAC (Fig. 6c). Additionally, small-intestinal sections from mice exposed to chemotherapy and radiotherapy showed greater loss of crypt villus structure and a significant reduction in crypt depth and number, as well as villus height and length, compared with normal mice. In contrast, mice that received NecroX-7 had well-formed crypts and a normal villus height. Furthermore, the protective effects of NecroX-7 were more marked than those of NAC (Fig. 6d–f). We also evaluated cell death and mitochondrial ROS production in intestinal epithelial cells (Supplementary Figure 1) and keratinocytes (data not shown) subjected to 5-FU treatment using CCK-8 and MitoTracker-ROS. NecroX-7 exerted a significantly greater suppressive effect on apoptosis and mitochondrial ROS production than NAC. This suggests that antioxidants that target mitochondria have therapeutic potential for OM.

NecroX-7 does not affect radiation- or chemotherapy-induced tumor regression

OM is a side effect of radiotherapy and chemotherapy. Thus, to confirm the efficacy of an anti-mucositis agent, its effect on tumor proliferation should be evaluated. Therefore, we examined the effect of NecroX-7 on the antitumor activity of 5-FU in mice implanted with tumors composed of murine colon cancer MC-38 cells (Fig. 7a). Mice were injected subcutaneously (s.c.) with MC-38 cells and started 5-FU treatment 9 days later (when the tumor became visible). The 5-FU dose used was the minimum (20 mg/kg for 5 days) required to reduce MC-38 tumor growth without lethality for at least 13 days from the start of treatment. Administration of NecroX-7 did not affect tumor growth (Fig. 7b), and 5-FU both with or without NecroX-7 decreased the tumor volume. We also investigated the effects of NecroX-7 on sensitivity to radiotherapy in tumor growth. Mice were injected s.c. with MC-38 cells on day 0, followed by TBI at 1100 rad and syngeneic bone marrow transplantation (BMT) on day 9. As shown in Fig. 7c, there was no difference in tumor growth between the group that received syngeneic BMT together with NecroX-7 injection and the group that received syngeneic BMT alone. These results suggest that NecroX-7 does not modulate the antitumor activity of

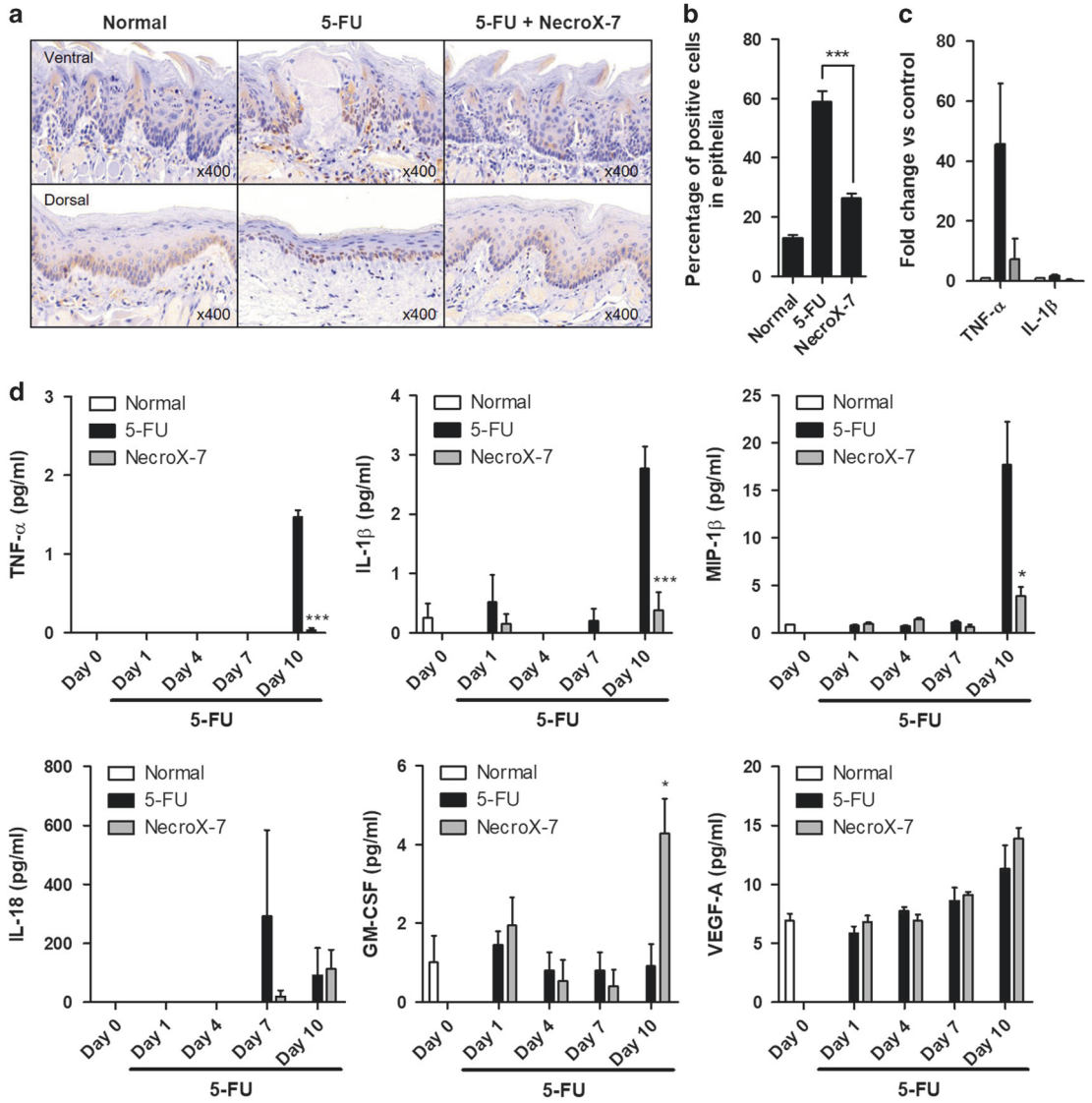

Fig. 5 Effect of NecroX-7 on inflammation in mice with oral mucositis. **a** Representative immunohistochemical staining for nuclear factor-κB (NF-κB) subunit p65 in the tongue on day 10. Original magnification, ×400. **b** Quantification of the nuclear NF-κB subunit p65 in **a**. **c** Tumor necrosis factor-alpha (TNF-α) and interleukin (IL)-1β expression levels in tongue tissues were determined by real-time polymerase chain reaction using β-actin for normalization. **d** Serum TNF-α, IL-1β, MIP-1β, IL-18, granulocyte-macrophage colony-stimulating factor (GM-CSF), and vascular endothelial growth factor-A (VEGF-A) levels were measured by enzyme-linked immunosorbent assay on day 10. N7 NecroX-7. *P < 0.05, ***P < 0.001

both 5-FU and radiation. Therefore, NecroX-7 shows potential for treatment of OM in patients undergoing anticancer treatment.

AAV9-mediated HMGB1 overexpression exacerbated mucosal injury and inflammation by chemotherapy

To further determine whether HMGB1 can directly promote chemotherapy-induced OM, we utilized the AAV9-vector system (AAV9-CMV-HMGB1-Luc) to establish an HMGB1 overexpression animal model (Supplementary Figure 2a). AAV-Mock-Luc (Luc) or AAV-HMGB1-Luc (HMGB1) packaged in AAV9 capsids were administered to 5-week-old mice by i.v. injection. Two weeks after i.v. injection, we observed the systemic gene delivery efficiency and tissue tropism of AAV9 through ex vivo bioluminescence imaging. Representative bioluminescent images of AAV-HMGB1-Luc-infected mice are shown in Fig. 8a. Luciferase expression in mice injected with HMGB1-Luc was mainly present in the tongue tissues, liver, and gut, and manifested to a lesser extent in the spleen, heart, and kidney (Supplementary Figure 2a). Overexpression of HMGB1 was confirmed in the tongue tissues of AAV-HMGB1-Luc-infected mice compared with those infected with AAV-Mock-Luc (Fig. 8b). These AAV-infected mice were then used to generate a 5-FU-induced mouse model of OM following the protocol illustrated in Fig. 8c. Interestingly, 5-FU-triggered mucosal injury (toluidine blue; Fig. 8d, e) and epithelial cell death (TUNEL; Fig. 8f, g), and the inflammatory microenvironment, including NF-κB pathway activation (Fig. 8k), were exacerbated in AAV-HMGB1-infected mice compared with the AAV-Mock-infected control group. A similar pattern was observed in the significant decrease in mucosal basal epithelial layer thickness (H & E; Fig. 8h, i) and proliferation of epithelial cells (Ki67; Fig. 8j). In addition, increased expression of TNF-α and IL-1β in the tongue tissues of the 5-FU-treated AAV-HMGB1-infected mice was confirmed through PCR (Fig. 8l, m). These results clearly demonstrate that HGMB1 promotes basal layer epithelial cell death and inflammation in OM during chemotherapy and plays a key role in the pathogenesis of OM.

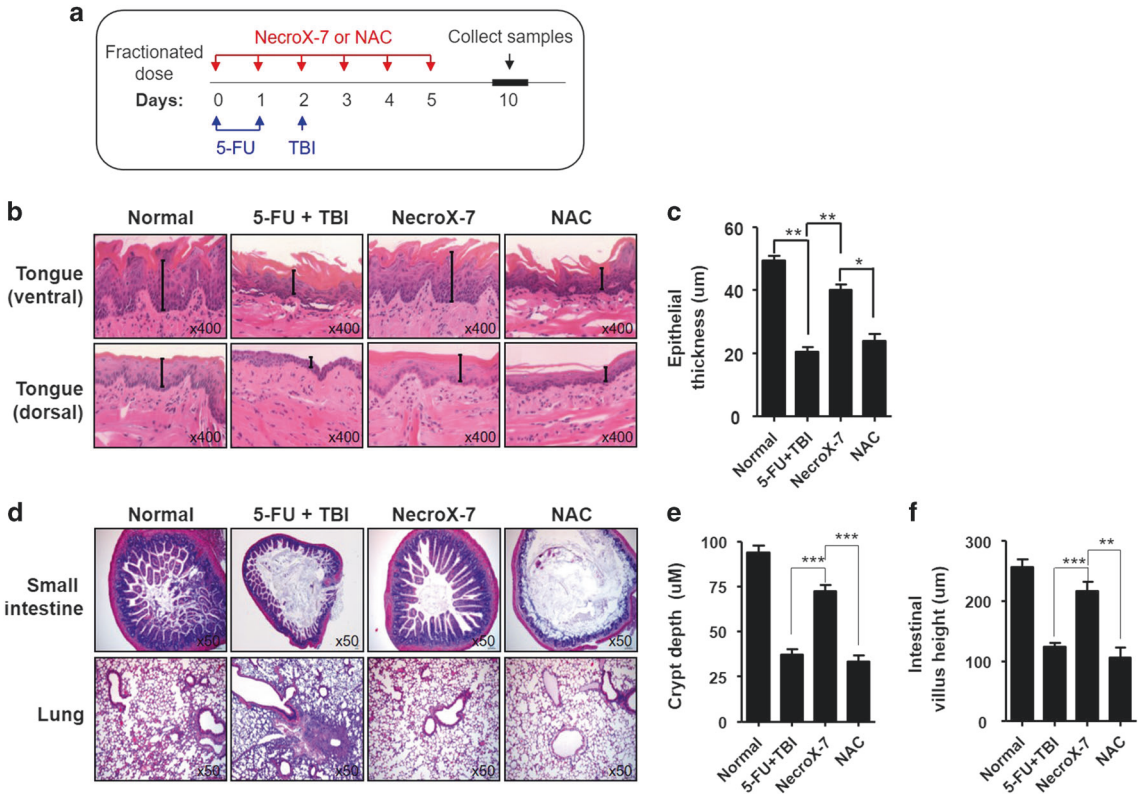

Fig. 6 Effect of NecroX-7 on the oral and intestinal mucosa of mice receiving 5-fluorouracil (5-FU) and total body irradiation (TBI). **a** Experiment protocol. Oral and gastrointestinal mucositis were induced in mice using 5-FU (50 mg/kg, qdx2), followed by TBI (8 Gy, single fraction). NecroX-7 (30 mg/kg, intravenous) or phosphate-buffered saline was administered once daily for 5 days. Morphological changes were evaluated by hematoxylin and eosin (H & E) staining on day 10 after initiation of 5-FU and TBI. **b** Representative H & E-stained micrographs of the dorsal (upper panel) and ventral (lower panel) tongue. Original magnification, ×400. **c** Tongue mucosal epithelium thickness. **d** H & E-stained images of mouse small intestine (upper panel) and lung (lower panel). Original magnification, ×50. **e** Crypt depth and **f** intestinal villus height. NAC *N*-acetylcysteine, N7 NecroX-7. Results are representative of two independent experiments ($n = 5–6$ mice/group). $^{*}P < 0.05$, $^{**}P < 0.01$, $^{***}P < 0.001$

DISCUSSION

Oxidative stress is a key mediator of the initiation of OM, directly damages cells, tissues, and blood vessels, and activates the biologic pathways that lead to an acute tissue response.[30] We hypothesized that HMGB1 plays a key role in this process. In the current study, we observed mucosal basal layer epithelial cell death and loss of membrane integrity in the tongue tissue of mice that received high-dose anticancer treatment (Fig. 1), and continuous HMGB1 release (Fig. 3). These data confirm the correlation between HMGB1 release and increased severity of OM. Consequently, we suggest that HMGB1 may be an independent predictor of OM severity, and a target for the treatment of OM.

We clearly demonstrated that HMGB1 overexpression exacerbates chemotherapy-induced mucosal injury and inflammatory responses including the NF-κB pathway (Fig. 8). This finding suggests that in OM-inducing environments characterized by exposure to high-dose anticancer agents, excessive HMGB1 accumulation induces cell death and inflammation and suppresses regeneration and stem cell repair (Fig. 9). In contrast to our findings, recent studies reported that HMGB1 from epithelial cells, proposed to induce epithelial–mesenchymal transition and cell migration through β-catenin pathways,[31] resulted in protection of the intestinal mucosa from damage.[32] These contradictory findings may be ascribed to different functions in the context of various disease states.

Previous studies have suggested that the biological activity of HMGB1 is largely determined by the redox state. Fully reduced HMGB1 forms are able to bind abundant chemokine CXCL12 and retain the ability to signal through CXCR4 and orchestrate hematopoietic, liver,[33] and muscle regeneration.[34,35] In contrast, it has been reported that disulfide HMGB1 has pro-inflammatory cytokine-inducing properties resulting from TLR4-MD-2 responses[36] and that terminally oxidized sulfonyl HMGB1 lacks inflammatory activity properties.

Although we suggest that excessive HMGB1 accumulation induces cell death and inflammation in chemoradiotherapy-associated mucositis, it is necessary to conduct a careful assessment for various disease states and samples to determine the precise role of HMGB1. In further studies, we will explore the clinical implications of HMGB1 isoforms in patients receiving chemotherapy or HSCT.

In this study, we showed that NecroX-7, which suppresses HMGB1 secretion, could be used to treat OM caused by chemotherapy, and assessed its efficacy in several animal models. Indeed, NecroX-7 alleviated OM in mice subjected to cancer treatment (Fig. 1), which was related to suppression of HMGB1 release (Fig. 3). In addition, NecroX-7 suppressed cytoplasmic NF-κB translocation, which represents the link between the inflammatory response with mucosal injury, as well as TNF-α, IL-1β, and MIP-1 expression (Fig. 5).

A study involving TLR-knockout mice and TLR agonists demonstrated that the innate immune system plays a key role in the pathophysiology of OM. TLR3−/− mice exhibited strong resistance to radiation-induced cell death,[37] and injection of the TLR 2, 4, and 5 agonists lipopolysaccharide,[38] *Lactobacillus*,[39] and flagellin[19,39] resulted in radioprotective effects. However, therapeutic application of TLR agonists is limited by the risk of

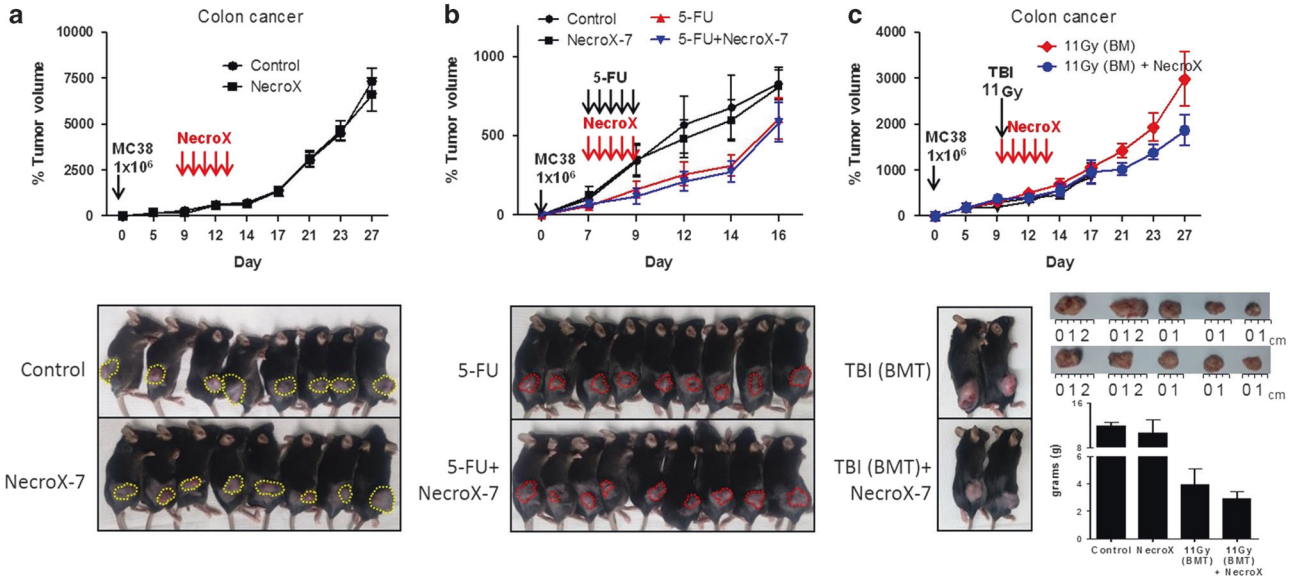

Fig. 7 Antitumor effect of NecroX-7 alone or in combination with 5-fluorouracil (5-FU). **a** C57BL/6 mice were administered 10^6 MC-38 tumor cells subcutaneously (s.c.) and treated from days 9 to 13 with (red) NecroX-7 or (black) phosphate-buffered saline (PBS) as a control. Tumor size was measured every 2–4 days starting on day 5. Data are representative of two independent experiments with at least 5 mice/group. **b** C57BL/6 mice were administered 10^6 MC-38 tumor cells s.c. On day 7, 20 mice were randomly divided into four groups, and were administered (red) 5-FU (20 mg/kg, i.p.) from days 7 to 11 followed by (blue) NecroX-7 (30 mg/kg, intravenous (i.v.)) once daily for 5 days, starting 7 days after implantation. Tumor size was measured every 2–3 days starting on day 7. Data are representative of two independent experiments with at least 5 mice/group. **c** C57BL/6 mice were administered 10^6 MC-38 tumor cells s.c. and 1100 cGy total body irradiation and syngeneic bone marrow transplantation (5×10^6 cells, i.v.) on day 9, followed by (blue) NecroX-7 or (red) PBS as a control from days 9 to 13. Tumor size was measured every 2–4 days starting on day 5. N7 NecroX-7. Data are representative of two independent experiments with at least 5 mice/group

exacerbating the inflammatory responses associated with OM. NecroX-7 prevented the suppressed proliferation of epithelial cells caused by chemotherapy-induced mucosal injury, and reduced secondary inflammatory responses. Thus, NecroX-7 has potential in the treatment of OM.

In a clinical study of 212 hematologic cancer patients, palifermin was reported to reduce the duration and severity of OM occurring after intensive chemotherapy and radiotherapy.[40] In particular, the therapeutic efficacy of palifermin was confirmed in a phase II clinical study[41] and the drug was approved by the FDA for "prevention of OM caused by anticancer treatment". Despite the therapeutic effects of growth factors, including palifermin, their clinical application is limited[42] due to the risk of promoting cancer cell growth. As such, issues related to cancer must be taken into consideration during the development of anti-OM drugs. In this study, we found that NecroX-7 suppresses cancer cell proliferation. In addition, the antitumor activity of 5-FU was not affected by administration of NecroX-7 in vivo (Fig. 7). The expression of Treg-related transcription factors (Foxp3) was not increased in tongue tissues of this mouse (data not shown).

NecroX is based on an indole moiety, a different substitution pattern structure consisted of benzene and pyrrole rings. NecroX-7 is a privileged structure compound in which the 7-position of the indole nucleus is chain-modified (Supplementary Figure 1a). These characteristics enable NecroX-7 to penetrate the mitochondrial matrix (data not shown). In addition, experiments using various redox-sensitive fluorescent probes (DCFDA, DHR123, and CH-H_2XROS) showed that NecroX-7 suppresses the accumulation of ROS and reactive nitrogen species. Antioxidant agents have been subjected to clinical trials;[11,43,44] however, these have shown limited efficacy in OM patients as the antioxidant agents cannot penetrate mitochondria in vivo. In contrast, NecroX-7 prevents ROS accumulation within the mitochondrial matrix. Therefore, NecroX-7 may have greater efficacy against OM than existing antioxidant agents.

In this study, we focused on chemoradiotherapy-induced mucosal toxicity, in particular, oral mucosal injury; however, mucositis can occur anywhere along the entire digestive tract from mouth to anus.[45,46] Using our mucositis model, we induced oral mucosal injury and gastrointestinal damage, including intestinal hemorrhaging and fecal incontinence (Supplementary Figure 3). These findings are consistent with previous observations that 5-FU induces gastrointestinal mucositis.[47] We also confirmed the increase in HMGB1 in small intestine tissues following 5-FU treatment and the protective effects of NecroX-7 against gastrointestinal mucosal injury by effectively inhibiting HMGB1 release (Supplementary Figures 3, 4). This finding implies that HMGB1 acts as a mechanism similar to OM pathogenesis and can be a key mediator in GI mucositis. However, as our pathological evaluations determined that small intestine mucosal layer injury was more aggressive than oral mucosal injury, further studies should be conducted on GI pathogenesis.

In conclusion, our data suggest that NecroX-7 suppresses HMGB1 release and downregulates the PUMA/p53 signaling pathway, resulting in amelioration of OM induced by chemotherapy and/or radiation (Fig. 9). Our data also indicate the potential of HMGB1 as a marker for diagnosis and prediction of the treatment response of OM. Further studies are needed to confirm the efficacy of HMGB1 in OM patients. Moreover, the correlation between HMGB1 and the development of OM should be confirmed in patients undergoing chemotherapy or HSCT (ClinicalTrials.gov identifier, NCT02044185).

METHODS

Materials

NecroX-7 ($C_{25}H_{32}N_4O_4S_2$; molecular weight, 516.67 Da; patent number, KR2008-0080519) was provided by LG Chem (previously LG Life Sciences, Korea). Monochlorobimane was obtained from Molecular Probes (Eugene, OR, USA); all other chemicals used were from Sigma-Aldrich (St. Louis, MO, USA).

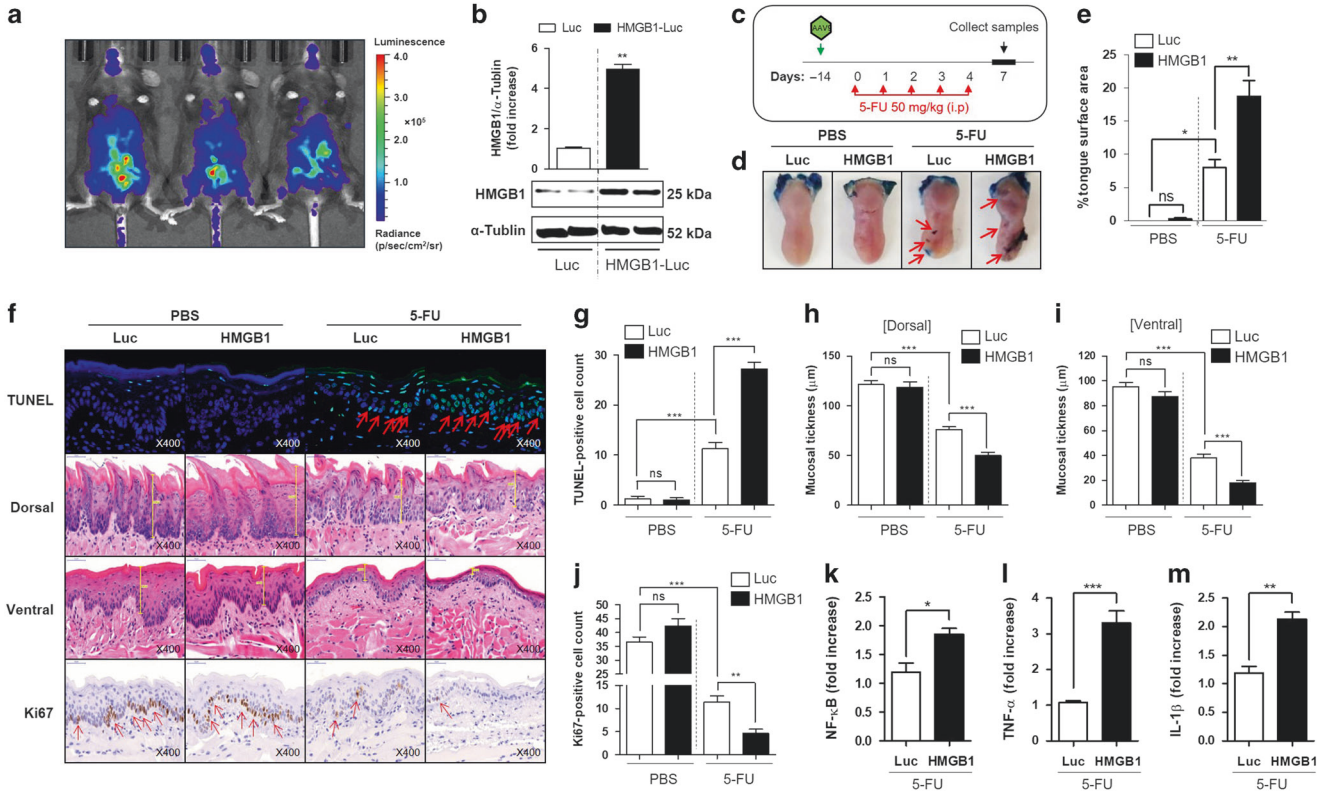

Fig. 8 High-mobility group box 1 (HMGB1) overexpression in mice infected with AAV9-HMGB1-Luc aggravated increased mucosal injury and inflammation in 5-fluorouracil (FU) induced mucositis model. AAV vectors were packaged into AAV9 capsids. Mice were injected with the indicated AAV vector (5×10^{11} viral genomes/mouse) via intravenous. **a** In vivo bioluminescence images of an AAV-HMGB1-Luc-infected mouse obtained on day 14, following vector administration. Images were acquired using a Xenogen IVIS imaging system. **b** Western blot analysis of HMGB1 expression in tongue tissues of AAV9-HMGB1-Luc-infected or AAV9-Mock-Luc-infected mice. HMGB1 protein levels in tongue tissues were increased in AAV9-HMGB1-Luc-infected mice compared with AAV9-Luc mice. **c** Experimental setup for mice infected with AAV9-HMGB1-Luc or AAV9-Mock-Luc and subsequent mouse model of mucositis. **d** Tongues from phosphate-buffered saline (PBS)- or 5-FU-treated AAV-Mock or AAV-HMGB1-infected HMGB1 overexpression mice were stained with toluidine blue. Arrow points to surface lesion. **e** Bar graph shows percentage of toluidine blue-stained surface in each mouse. **f** Paraffin tissue sections of tongue tissues were stained with terminal deoxynucleotidyl transferase-dUTP nick-end labeling (TUNEL; upper panel), hematoxylin and eosin (middle panel), and Ki67 (lower panel). Original magnification, ×400. **g** Quantification (mean ± standard deviation (SD)) of the TUNEL-positive cell count in **f**. **h**, **i** Mucosal thickness in mouse dorsal and ventral tongue. **j** Quantification (mean ± SD) of the Ki67-positive cell count in **f**. **k**–**m** Real-time PCR analysis of nuclear factor-κB (NF-κB), tumor necrosis factor-alpha (TNF-α), and interleukin-1β (IL-1β) cytokines in tongue tissues. Results are representative of two independent experiments ($n = 5$–8 mice/group). *$P < 0.05$, **$P < 0.01$, ***$P < 0.001$

Animals

Five- to 8-week-old female C57BL/6 mice were purchased from OrientBio (Sungnam, Korea). The mice were maintained under specific pathogen-free conditions in an animal facility with a controlled humidity of 55% (±5%), a 12/12 h light/dark cycle, and a temperature of 22 °C (±1 °C). The air in the animal facility was passed through a HEPA filter system. Animals were provided with mouse chow and tap water ad libitum. The study protocols were approved by the Animal Care and Use Committee of the Catholic University of Korea.

Mucositis models

Mice were administered 5-FU (50 mg/kg, Sigma-Aldrich) intraperitoneally (i.p.) once daily for 5 days (days 0–4), and saline (the vehicle for 5-FU) was administered to normal animals. NecroX-7 (0.3, 3, and 30 mg/kg) was administered intravenously (i.v.) daily for 5 days (days 0–4), and saline (the vehicle for NecroX-7) was administered to control animals. The doses of NecroX-7 were chosen based on our previous study[25]. Mice were euthanized 1, 4, 7, and 10 days after initiation of injection of 5-FU, and tongue and intestine tissues were collected for further analysis.

Clinical score

The severity of diarrhea and body weight loss was monitored throughout the experimental periods. Diarrhea severity was scored as described by Kurita et al.[48,49] as follows: 0, normal or absent stool; 1, slight, slightly wet, and soft stool; 2, moderate, wet, and unformed stool with perianal staining of the coat; and 3, severe, watery stool with perianal staining of the coat.

Macroscopic and histopathologic examination

Tongues were stained with 1% toluidine blue in 10% acetic acid for 1 min, followed by repeated washes with acetic acid, to reveal surface erosive or ulcerative lesions.[50] The percentage of toluidine blue-positive surface area was calculated using ImageJ software. Tissues were formalin-fixed, paraffin-embedded, and sectioned at a thickness of 4 μm. Ulcer size and mucosal epithelial thickness in tongues and villus length in the small intestine were measured in H & E-stained tissues using Panoramic Viewer software.

TUNEL assay and immunohistochemistry

Tissues were formalin-fixed, paraffin-embedded, and sectioned at a thickness of 3 μm. Staining for TUNEL assay was performed using the Click-iT Plus TUNEL assay kit (Invitrogen; Thermo Fisher

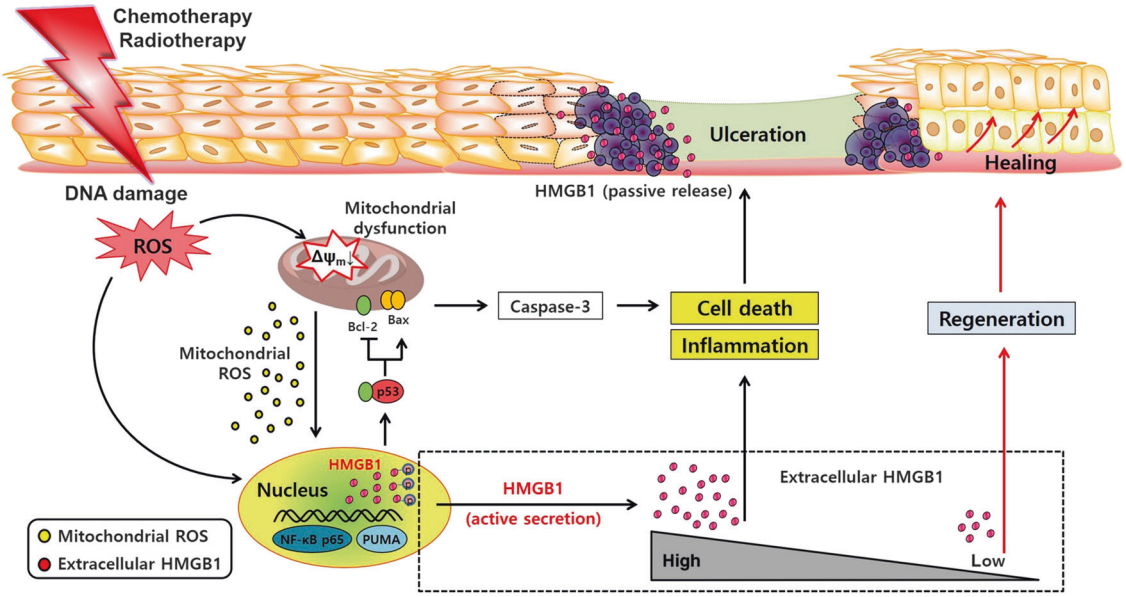

Fig. 9 Protective effect of NecroX-7 against chemo- and radiotherapy-induced oral mucositis (OM). Chemo- or radiotherapy-induced OM is initiated by direct injury to basal layer epithelial cells. These cells experience DNA damage and increased reactive oxygen species (ROS) levels, leading to mitochondrial dysfunction. Increased ROS levels in mitochondria trigger translocation of high-mobility group box 1 (HMGB1) from the nucleus to the cytoplasm, followed by its secretion extracellularly. A high level of HMGB1 triggers production of pro-inflammatory cytokines and activates the nuclear factor-κB pathway, resulting in development of OM. Therefore, HMGB1 has potential as a target for treatment of OM. Because NecroX-7 administration reduces mitochondrial ROS levels and blocks HMGB1 secretion, little HMGB1 remains in the mucosal tissue. This reduced HMGB1 level promotes cell regeneration and repair, which ameliorates OM

Scientific, Inc.) according to the manufacturer's protocol. For immunohistochemistry, slides were dehydrated using xylene and ethanol, and antigen retrieval and blocking were performed. Sections were further labeled with HMGB1 (1:250, Abcam [Cambridge, UK], 79823) or ki67 (1:200, Cell Signaling Technology, 16667), p53 (1:100, Abcam, 131442), or NF-κB p65 (1:800, Cell Signaling Technology, 8242) primary antibodies overnight at 4 °C. Anti-rabbit IgG-HRP (Santa Cruz Biotechnology) was used as the secondary antibody, and slides were incubated at room temperature for 2 h. Signals were detected using the REAL EnVision detection system, peroxidase/DAB+ (Dako, Santa Clara, CA, USA). Counterstaining was performed using Mayer's hematoxylin (Dako) for 1 min at room temperature.

Western blot

Total protein was prepared from freshly isolated tongue tissue, and western blotting was performed. The primary antibodies used were rabbit antibodies to PARP and cleaved PARP (1:1000, Cell Signaling Technology [Danvers, MA, USA], 9542), HMGB1 (1:50,000, Abcam [Cambridge, UK], 79823), phospho-p53 (1:1000, Cell Signaling Technology, 9284), p53 (1:500, Abcam, 131442), and α-tubulin (1:1000, Cell Signaling Technology, 2144). After an appropriate incubation, the horseradish peroxidase (HRP)-conjugated secondary antibody was added. After washing with Tris-buffered saline and Tween 20, the hybridized bands were detected using an enhanced chemiluminescence (ECL) detection kit and Hyperfilm-ECL reagents (Amersham Pharmacia Biotech).

Real-time reverse transcription-PCR

Total RNA was extracted using the TRIzol-LS reagent (Invitrogen). Total RNA (2 μg) was reverse-transcribed at 50 °C for 2 min, followed by 60 °C for 30 min. Quantitative PCR was performed using the FastStart DNA Master SYBR Green I kit and a LightCycler 480 Detection system (both from Bio-Rad, Hercules, CA, USA), as specified by the manufacturer. The crossing point was defined as the maximum of the second derivative from the fluorescence curve. Negative controls were included and contained all elements of the reaction mixture except for template DNA. For quantification, we report relative mRNA levels of specific genes obtained using the $2^{-\Delta Ct}$ method and used the β-actin housekeeping gene for normalization. The primers used are shown in Supplemental Table 1.

Luminex multiplex cytokine assay

Serum concentrations of the following immune molecules were determined using a magnetic bead-based 6-plex immunoassay: TNF-α, IL-1β, MIP-1β, IL-18, GM-CSF, and VEGF-A (customized Procartaplex, Thermo Scientific, USA). Serum samples were obtained from mice and run in duplicate along with serial standards and buffer controls. The median fluorescence intensity of analytes was detected using the flow-based MAGPIX System (Merck Millipore). Cytokine concentrations were calculated using Luminex xPONENT v. 4.2 software using a standard curve derived from known reference concentrations supplied by the manufacturer. A five-parameter model was used to calculate final concentrations by interpolation. Values are expressed in pg/mL.

MC-38 tumor induction

Mice were injected s.c. in the shaved right flank with MC-38 cells (1×10^6/200 μL). When the tumor had grown to 0.1–0.2 cm (palpable tumor, routinely on day 9), mice were injected i.p. with 200 μL of 5-FU (20 mg/kg for 5 days) or 1100 cGy TBI and syngeneic BMT (5×10^6 cells, i.v.). Tumor size was monitored daily using calipers and expressed as means ± SEM.

AAV vector packaging, purification, and titration

The AAV-Luc vector, obtained directly from Vector Biolabs Inc. (Malvern, PA, USA), contains the gene for luciferase under the transcriptional control of the cytomegalovirus immediate–early promoter (CMV promoter). The AAV-HMGB1 expression vector was generated by inserting m-HMGB1 ORF (BC083067) into the primary AAV-CMV-MCS-IRES-Luc plasmid. To package AAV vectors, HEK293T cells were transfected with AAV-HMGB1-Luc or AAV-Luc plasmids and helper plasmid together with AAV9 capsid plasmid

(Vector Biolabs Inc.). After 48 h, cells were collected and AAV vectors were purified using the AAV Purification Kit (Vector Biolabs Inc.) according to the manufacturer's instructions. Viral genomic copies were determined by measuring the viral nucleic acid content of affinity-purified AAV particles using the Quick Titer AAV Quantitation Kit.

Statistical analysis

Data are presented as means ± SD. Comparisons between two groups and more than two groups were performed by the Mann–Whitney *U* test or Student's *t*-test and the Kruskal–Wallis test, respectively. To assess the Gaussian distribution and equality of variance, the Shapiro-Wilk test and Levene test, respectively, were used. Statistical analysis was performed using the SPSS statistical software package (ver. 16.0; SPSS, Chicago, IL, USA). *P*-values < 0.05 were considered to indicate significance.

ACKNOWLEDGEMENTS

This work was supported by Grant HI14C3417 from the Korea Healthcare Technology Research and Development Project, Ministry for Health, Welfare, and Family Affairs, Republic of Korea.

AUTHOR CONTRIBUTIONS

K.-I.I., conception and design, data analysis and interpretation, manuscript writing; Y.-S.N., collection and/or assembly of data; N.K., collection and/or assembly of data, data analysis and interpretation; Y.S., collection and/or assembly of data; E.-S.L., collection and/or assembly of data; J.-Y.L., collection and/or assembly, analysis, and interpretation; Y.-W.J., conception and design, administrative support; S.-G.C., conception and design, data analysis and interpretation, administrative support, and final approval of manuscript.

ADDITIONAL INFORMATION

The online version of this article (https://doi.org/10.1038/s41385-019-0132-x) contains supplementary material, which is available to authorized users.

Competing interests: The authors declare no competing interests.

Publisher's note: Springer Nature remains neutral with regard to jurisdictional claims in published maps and institutional affiliations.

REFERENCES

1. Sonis, S. T. The pathobiology of mucositis. *Nat. Rev. Cancer* **4**, 277–284 (2004).
2. Sonis, S. T. Pathobiology of oral mucositis: novel insights and opportunities. *J. Support Oncol.* **5**, 3–11 (2007).
3. Henke, M. et al. Palifermin decreases severe oral mucositis of patients undergoing postoperative radiochemotherapy for head and neck cancer: a randomized, placebo-controlled trial. *J. Clin. Oncol.* **29**, 2815–2820 (2011).
4. Le, Q. T. et al. Palifermin reduces severe mucositis in definitive chemoradiotherapy of locally advanced head and neck cancer: a randomized, placebo-controlled study. *J. Clin. Oncol.* **29**, 2808–2814 (2011).
5. Kim, K. A. et al. Mitogenic influence of human R-spondin1 on the intestinal epithelium. *Science* **309**, 1256–1259 (2005).
6. Zhao, J. et al. R-Spondin1 protects mice from chemotherapy or radiation-induced oral mucositis through the canonical Wnt/beta-catenin pathway. *Proc. Natl Acad. Sci. USA* **106**, 2331–2336 (2009).
7. Zhou, W. J., Geng, Z. H., Spence, J. R. & Geng, J. G. Induction of intestinal stem cells by R-spondin 1 and Slit2 augments chemoradioprotection. *Nature* **501**, 107–111 (2013).
8. Iglesias-Bartolome, R. et al. mTOR inhibition prevents epithelial stem cell senescence and protects from radiation-induced mucositis. *Cell Stem Cell* **11**, 401–414 (2012).
9. Wei, L. et al. Inhibition of CDK4/6 protects against radiation-induced intestinal injury in mice. *J. Clin. Investig.* **126**, 4076–4087 (2016).
10. Yan, K. S. et al. The intestinal stem cell markers Bmi1 and Lgr5 identify two functionally distinct populations. *Proc. Natl Acad. Sci. USA* **109**, 466–471 (2012).
11. Hwang, W. Y. et al. A randomized trial of amifostine as a cytoprotectant for patients receiving myeloablative therapy for allogeneic hematopoietic stem cell transplantation. *Bone Marrow Transplant.* **34**, 51–56 (2004).
12. Han, G. et al. Preventive and therapeutic effects of Smad7 on radiation-induced oral mucositis. *Nat. Med.* **19**, 421–428 (2013).
13. Lotze, M. T. et al. The grateful dead: damage-associated molecular pattern molecules and reduction/oxidation regulate immunity. *Immunol. Rev.* **220**, 60–81 (2007).
14. Rubartelli, A. & Lotze, M. T. Inside, outside, upside down: damage-associated molecular-pattern molecules (DAMPs) and redox. *Trends Immunol.* **28**, 429–436 (2007).
15. Akira, S., Uematsu, S. & Takeuchi, O. Pathogen recognition and innate immunity. *Cell* **124**, 783–801 (2006).
16. Vasconcelos, R. M. et al. Host-microbiome cross-talk in oral mucositis. *J. Dent. Res* **95**, 725–733 (2016).
17. Harris, H. E., Andersson, U. & Pisetsky, D. S. HMGB1: a multifunctional alarmin driving autoimmune and inflammatory disease. *Nat. Rev. Rheumatol.* **8**, 195–202 (2012).
18. Wang, H., Yang, H. & Tracey, K. J. Extracellular role of HMGB1 in inflammation and sepsis. *J. Intern. Med.* **255**, 320–331 (2004).
19. Kang, R. et al. HMGB1 in cancer: good, bad, or both? *Clin. Cancer Res.* **19**, 4046–4057 (2013).
20. Lotze, M. T. & Tracey, K. J. High-mobility group box 1 protein (HMGB1): nuclear weapon in the immune arsenal. *Nat. Rev. Immunol.* **5**, 331–342 (2005).
21. Kim, H. J. et al. NecroX as a novel class of mitochondrial reactive oxygen species and ONOO(-) scavenger. *Arch. Pharm. Res.* **33**, 1813–1823 (2010).
22. Gaiha, G. D. et al. Dysfunctional HIV-specific CD8 + T cell proliferation is associated with increased caspase-8 activity and mediated by necroptosis. *Immunity* **41**, 1001–1012 (2014).
23. Roca, F. J. & Ramakrishnan, L. TNF dually mediates resistance and susceptibility to mycobacteria via mitochondrial reactive oxygen species. *Cell* **153**, 521–534 (2013).
24. Kim, S. et al. Pharmacokinetics and safety of a single dose of the novel necrosis inhibitor LC28-0126 in healthy male subjects. *Br. J. Clin. Pharmacol.* **83**, 1205–1215 (2017).
25. Im, K. I. et al. The free radical scavenger NecroX-7 attenuates acute graft-versus-host disease via reciprocal regulation of Th1/regulatory T cells and inhibition of HMGB1 release. *J. Immunol.* **194**, 5223–5232 (2015).
26. Sonis, S. T. New thoughts on the initiation of mucositis. *Oral Dis.* **16**, 597–600 (2010).
27. Khoo, K. H., Verma, C. S. & Lane, D. P. Drugging the p53 pathway: understanding the route to clinical efficacy. *Nat. Rev. Drug Discov.* **13**, 217–236 (2014).
28. Qiu, W. et al. PUMA regulates intestinal progenitor cell radiosensitivity and gastrointestinal syndrome. *Cell Stem Cell* **2**, 576–583 (2008).
29. Villunger, A. et al. p53- and drug-induced apoptotic responses mediated by BH3-only proteins puma and noxa. *Science* **302**, 1036–1038 (2003).
30. Penayo, U., Caldera, T. & Jacobsson, L. [Prevalence of mental disorders in adults in Subtiava, Leon, Nicaragua]. *Bol. Oficina Sanit. Panam.* **113**, 137–149 (1992).
31. Chen, Y. C. et al. High mobility group box 1-induced epithelial mesenchymal transition in human airway epithelial cells. *Sci. Rep.* **6**, 18815 (2016).
32. Reed, K. R. et al. Secreted HMGB1 from Wnt activated intestinal cells is required to maintain a crypt progenitor phenotype. *Oncotarget* **7**, 51665–51673 (2016).
33. Hernandez, C. et al. HMGB1 links chronic liver injury to progenitor responses and hepatocarcinogenesis. *J. Clin. Investig.* **128**, 2436–2451 (2018).
34. Tirone, M. et al. High mobility group box 1 orchestrates tissue regeneration via CXCR4. *J. Exp. Med.* **215**, 303–318 (2018).
35. Lee, G. et al. Fully reduced HMGB1 accelerates the regeneration of multiple tissues by transitioning stem cells to GAlert. *Proc. Natl Acad. Sci. USA* **115**, e4463–e4472 (2018).
36. Yang, H. et al. MD-2 is required for disulfide HMGB1-dependent TLR4 signaling. *J. Exp. Med.* **212**, 5–14 (2015).
37. Takemura, N. et al. Blockade of TLR3 protects mice from lethal radiation-induced gastrointestinal syndrome. *Nat. Commun.* **5**, 3492 (2014).
38. Riehl, T., Cohn, S., Tessner, T., Schloemann, S. & Stenson, W. F. Lipopolysaccharide is radioprotective in the mouse intestine through a prostaglandin-mediated mechanism. *Gastroenterology* **118**, 1106–1116 (2000).
39. Ciorba, M. A. et al. Lactobacillus probiotic protects intestinal epithelium from radiation injury in a TLR-2/cyclo-oxygenase-2-dependent manner. *Gut* **61**, 829–838 (2012).
40. Spielberger, R. et al. Palifermin for oral mucositis after intensive therapy for hematologic cancers. *N. Engl. J. Med* **351**, 2590–2598 (2004).
41. Brizel, D. M. et al. Phase II study of palifermin and concurrent chemoradiation in head and neck squamous cell carcinoma. *J. Clin. Oncol.* **26**, 2489–2496 (2008).
42. Goldberg, J. D. et al. Palifermin is efficacious in recipients of TBI-based but not chemotherapy-based allogeneic hematopoietic stem cell transplants. *Bone Marrow Transplant.* **48**, 99–104 (2013).
43. Kamran, M. Z., Ranjan, A., Kaur, N., Sur, S. & Tandon, V. Radioprotective agents: strategies and translational advances. *Med. Res. Rev.* **36**, 461–493 (2016).

44. Moslehi, A. et al. N-acetyl cysteine for prevention of oral mucositis in hematopoietic SCT: a double-blind, randomized, placebo-controlled trial. *Bone Marrow Transplant.* **49**, 818–823 (2014).
45. Beck, P. L. et al. Chemotherapy- and radiotherapy-induced intestinal damage is regulated by intestinal trefoil factor. *Gastroenterology* **126**, 796–808 (2004).
46. Harris, D. J. Cancer treatment-induced mucositis pain: strategies for assessment and management. *Ther. Clin. Risk Manag.* **2**, 251–258 (2006).
47. Zhan, Y. et al. beta-Arrestin1 inhibits chemotherapy-induced intestinal stem cell apoptosis and mucositis. *Cell Death Dis.* **7**, e2229 (2016).
48. Guabiraba, R. et al. IL-33 targeting attenuates intestinal mucositis and enhances effective tumor chemotherapy in mice. *Mucosal Immunol.* **7**, 1079–1093 (2014).
49. Kurita, A. et al. Alleviation of side effects induced by irinotecan hydrochloride (CPT-11) in rats by intravenous infusion. *Cancer Chemother. Pharmacol.* **52**, 349–360 (2003).
50. Muanza, T. M. et al. Evaluation of radiation-induced oral mucositis by optical coherence tomography. *Clin. Cancer Res.* **11**, 5121–5127 (2005).